Research Article | Vol. 27, No. 15 | 22 Jul 2019 | OPTICS EXPRESS 20493
Optics EXPRESS

Design of lensless retinal scanning display with diffractive optical element

LANTIAN MI, CHAO PING CHEN,* YIFAN LU, WENBO ZHANG, JIE CHEN, AND NIZAMUDDIN MAITLO

Smart Display Lab, Department of Electronic Engineering, Shanghai Jiao Tong University, Shanghai, China
**ccp@sjtu.edu.cn*

Abstract: We propose a design of a retinal-scanning-based near-eye display for augmented reality. Our solution is highlighted by a laser scanning projector, a diffractive optical element, and a moist eye with gradient refractive indices. The working principles related to each component are comprehensively studied. Its key performance is summarized as follows. The field of view is 122°, angular resolution is 8.09′, diffraction efficiency is 57.6%, transmittance is 80.6%, uniformity is 0.91, luminance is 323 cd/m^2, modulation transfer functions are above 0.99999 at 3.71 cycle/degree, contrast ratio is 4878, and distortion is less than 24%.

1. Introduction

For a very long time, near-eye display (NED), also known as head-mounted display, remained as a marginal technology in the display community [1]. Until recently, in the wake of augmented and virtual realities [2], it theatrically morphs into a superstar sought after by a crowd of researchers, engineers, investors, bloggers etc. Technically, NED is a type of wearable projection display [3]. Pursuant to the criterion that whether the retina is the image plane, NED can be divided into two categories, *i.e.* indirect projection and direct or retinal projection. For the former, the image is first projected onto a virtual image plane, and then received by the retina. To do so, the optical path needs to be folded via either a combiner [4–11] or waveguide [12–22]. As far as the field of view (FOV) is concerned, both combiner and waveguide based NEDs have limited FOVs, usually below 50° [2]. Another restriction is the paradox that FOV is inversely proportional to the exit pupil [2]. There must be a trade-off between the FOV and exit pupil. Direct or retinal projection based NED, on the other hand, refers to the case when the image is directly projected to the retina, for which the image plane coincides with the retina. Virtual retinal display (VRD) [23–25], developed by Human Interface Technology Lab of University of Washington, is a pioneering retinal projection based NED, known for its concept of retinal scanning. iOptik [26,27], a proprietary technology of Innovega, is characterized by a contact lens embedded with a zone plate. Pinlight display [28], co-developed by University of North Carolina at Chapel Hill and Nvidia, mimics a pinhole camera by an array of point light sources in front of eye. Intel—through acquisitions of Composyt Light Labs and Lemoptix—built a smart glasses prototype dubbed Vaunt with holographic optical elements (HOEs) [29]. Though the above retinal projection based NEDs are able to achieve extremely large FOVs, each has its own pros and cons. The optical setup of VRD is bulky and sophisticated, making it unwearable. iOptik has been struggling for many years in persuading the consumers to wear the contact lens. Pinlight display is vulnerable to the change of eye state, including the diopter of eye, pupil size, and rotation of eyeball. Lasting for only 4 odd years, Vaunt was aborted in part due to manufacturability of HOEs. Inspired from the said issues, we would like to present a lensless retinal scanning display (RSD), which is compact in design and immune to the change in the pupil size and diopter of eye. In what follows, its structure, working principles, and overall performance are to be elaborated.

#365181 https://doi.org/10.1364/OE.27.020493
Journal © 2019 Received 16 Apr 2019; revised 22 Jun 2019; accepted 22 Jun 2019; published 9 Jul 2019

Optics EXPRESS

2. Principles

2.1 Proposed structure

The proposed RSD can be decomposed into three major components, *i.e.* a laser scanning projector, a diffractive optical element (DOE), and an eye, as shown in Fig. 1, where d_p is the distance between projector and glass, d_{doe} the distance between projector and DOE, d_{lens} the distance between DOE and lens center, W the horizontal dimension of DOE, x the distance starting from the left edge of DOE, θ_i the angle of incident light, and θ_m the angle of diffracted light. Inside the temple is housed the laser scanning projector for saving the room. On the inner surface of a flat glass substrate is fabricated the DOE, which is able to converge the light coming out of the projector towards the center of lens of eye. Analogous to the Maxwellian view [30], such configuration ensures that the image formed on the retina will remain intact no matter how the eye accommodates its diopter to the distance of object. Moreover, as long as the beam size of the laser is way smaller than the pupil—minimally 2 mm across [31]—the brightness of image could be maintained regardless of the variation of pupil size. For the sake of symmetry, the DOE and eye are center-aligned.

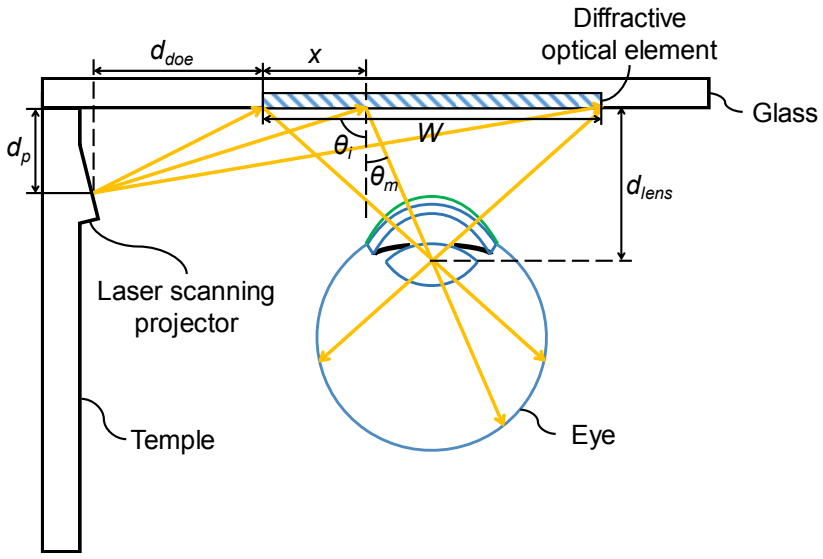

Fig. 1. Proposed structure of our RSD, which can be decomposed into three major components, *i.e.* a laser scanning projector, a DOE, and an eye. d_p is the distance between projector and glass, d_{doe} the horizontal distance between projector and DOE, d_{lens} the distance between DOE and lens center, W the dimension of DOE, x the distance starting from the left edge of DOE, θ_i the angle of incident light, and θ_m the angle of diffracted light.

2.2 Eye model

Unlike our previous eye models [32–34], in which the eye is dry—in the absence of tear—and lens of eye has a constant refractive index, the current model factors into not only the tear but also a gradient lens [35] studied by Goncharov *et. al*. Figure 2 is a cross-sectional view of our schematic moist eye, consisting of tear, cornea (anterior and posterior), aqueous chamber filled with aqueous humor, iris with an opening known as pupil, lens (anterior and posterior), vitreous chamber filled with vitreous humor, and retina. Approximately, two-thirds of the eye's optical power is derived from the cornea—including the tear—and one-third from the lens [36]. While the thickness of tear is negligibly thin—ranging from 6 to 20 μm—the irregularities of tear can cause significant visual aberrations and distortions [37].

Optics EXPRESS

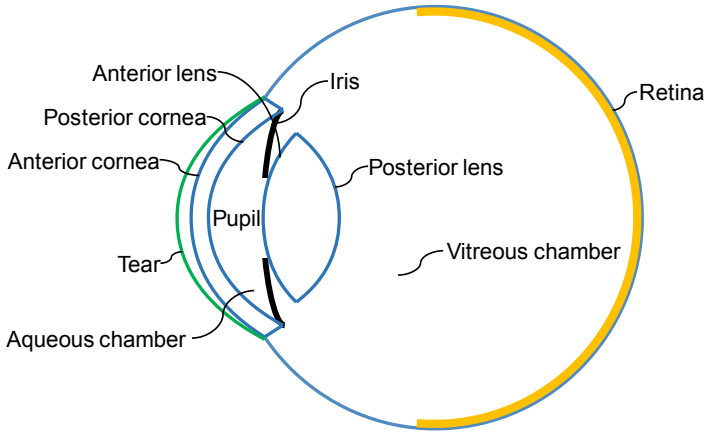

Fig. 2. Cross-sectional view of our schematic moist eye, consisting of tear, cornea (anterior and posterior), aqueous chamber filled with aqueous humor, iris with an opening known as pupil, lens (anterior and posterior), vitreous chamber filled with vitreous humor, and retina.

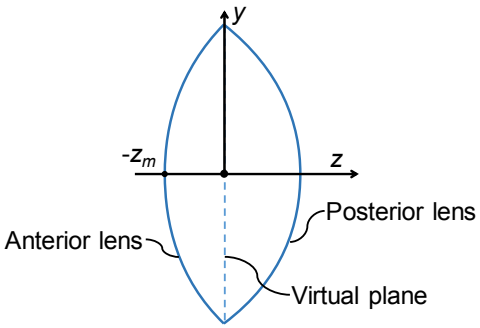

Fig. 3. Cross-sectional view of lens of eye with an assistive virtual plane. The center of virtual plane is designated as the center of lens. z is the distance measured from the vertex of anterior lens along the z-axis, and y the distance measured from the lens center along the y-axis.

To model the gradient lens, an assistive virtual plane is inserted to separate the lens into the anterior and posterior halves, as shown in Fig. 3. The center of lens is—coinciding with the nodal point [38]—designated as the origin of y-z coordinate. Invoking the Goncharov's gradient lens model [35], refractive indices n_a for the anterior lens and n_p for the posterior lens could be computed with

$$n_a(z,y) = n_{00} + c_{10}y^2 + c_{20}y^4 + c_{01}(z+z_m) + c_{02}(z+z_m)^2 + c_{03}(z+z_m)^3 + c_{04}(z+z_m)^4 \quad (1)$$

and

$$n_p(z,y) = n_{\max} + c_{10}y^2 + c_{20}y^4 + c_{01,2}z + c_{02,2}z^2 + c_{03,2}z^3 + c_{04,2}z^4 \quad (2)$$

respectively, where z is the distance measured from the vertex of anterior lens along the z-axis, y the distance measured from the lens center along the y-axis, z_m the distance between the vertex of anterior lens and the virtual plane, n_{00} the starting refractive index of anterior lens, n_{max} the maximum refractive index, and c_{10}, c_{20}, c_{01}, c_{02}, c_{03}, c_{04}, $c_{01,2}$, $c_{02,2}$, $c_{03,2}$, and $c_{04,2}$ the coefficients of each term. With the parameters disclosed in [35], which are itemized in Table 1, refractive indices of lens are calculated along the horizontal and vertical directions, respectively, as shown in Fig. 4. It can be seen that the refractive index maximizes at the lens center, from which it starts to decrease towards the outermost surface.

Optics EXPRESS

Table 1. Parameters of gradient lens

Coefficient	Value
n_{00}	1.376
z_m	2
c_{10}	–0.00174
c_{20}	1.88e-5
c_{01}	0.03996
c_{02}	–0.00998
c_{03}	0
c_{04}	0
n_{max}	1.416
$c_{01,2}$	0
$c_{02,2}$	–0.0108
$c_{03,2}$	–0.0018
$c_{04,2}$	–7.53e-5

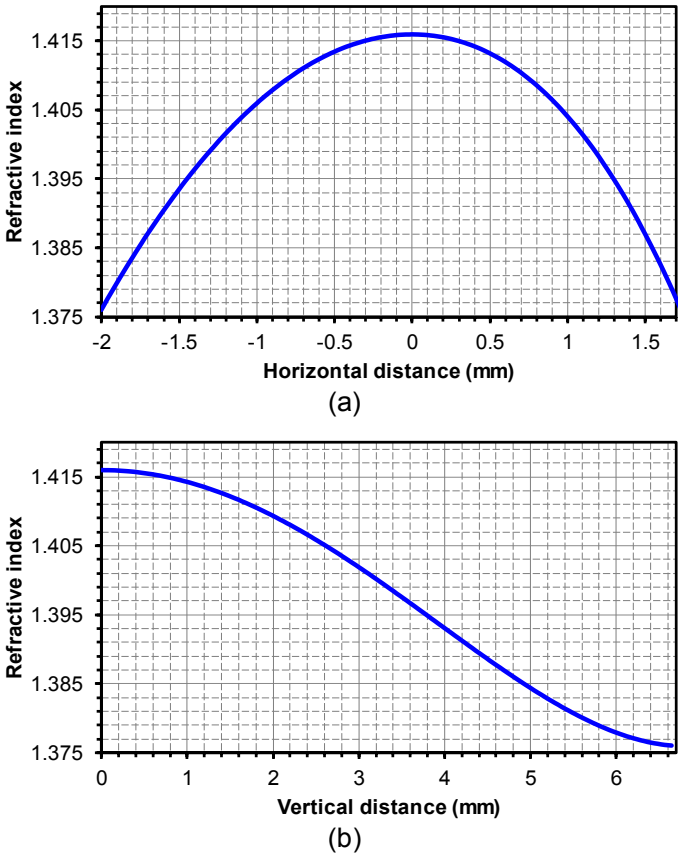

Fig. 4. Refractive indices of lens calculated along the (a) horizontal and (b) vertical directions, respectively. It can be seen that the refractive index maximizes at the center, from which it starts to decrease towards the outermost surface.

Optics EXPRESS

2.3 Laser scanning projector

Figure 5 is a schematic drawing of the laser scanning projector, inside which are mounted a laser diode, a circular polarizer, a mirror, and a scanning mirror controlled by a biaxial micro-electromechanical system (MEMS) [39]. Laser is transformed to circular polarization after passing through the circular polarizer. Since the laser scanning projector is lensless, the image projected onto the retina will be always in focus—in other words, its depth of focus is infinite—even when the eye is defocused. In this regard, the laser scanning projector is essentially a pinhole camera [40]. This is a big advantage over the lens-based projector, whose image plane is at a certain distance and depth of focus is finite [3]. The depth cue of the projected image, on that other hand, shall be coupled with the distance of real object, depending on the accommodation of eye [32]. A major downside of laser scanning projector, among others, is about its low resolution—*e.g.* the best resolution of Microvision's laser scanning projector is merely 848 × 480 [41]—restricted by the scanning rate of MEMS. Due to the limited choices of laser scanning projector available in the market, a set of parameters customized to our design are given in Table 2, where the resolution is 640 × 640, scanning angle (horizontal) is 17°, beam diameter at the waist D_0 is 0.4 mm, luminous flux Φ is 2 lm, and contrast ratio (CR) is 5000. Being treated as a Gaussian TEM_{00} beam, beam diameter D of the laser enlarges as it propagates at a distance L from the waist, which is described as [42]

$$D = D_0 \sqrt{1 + \left(\frac{4M^2 \lambda L}{\pi D_0^2} \right)^2} \tag{3}$$

where M^2 is the beam quality and λ is the wavelength of laser. The beam divergence θ_{div} is therefore

$$\theta_{div} = \frac{2M^2 \lambda}{\pi D_0} \tag{4}$$

For M^2 = 1.1, λ = 532 nm, L = 50 mm, and D_0 = 0.4 mm, D = 0.411 mm and θ_{div} = 0.93 mrad or 0.05°. As a rule of thumb, for a laser with a beam divergence less than 1 mrad, its beam can be approximated as the perfectly collimated one. Upon the reflection of MEMS, both the shape and size of the said laser beam will be altered. To match the shape and size of the subsequent DOE, MEMS is square in shape and 60 μm wide, as will be discussed later. To avoid the loss of light, a beam shaper could be inserted on top of the laser diode. Plus, in case the projector and DOE are misaligned during the mounting, it is suggested to make both of them adjustable for calibration. Incidentally, speaking of the speckle effect, a random laser made from disordered materials [43] is among the most desirable solutions.

Table 2. Parameters for laser scanning projector

Object	Parameter	Value
Laser scanning projector	*Resolution*	640 × 640
	Scanning angle (horizontal)	17°
	Beam quality	1.1
	Beam diameter (waist)	0.4 mm
	Divergence angle	0.93 mrad
	Luminous flux	2 lm
	CR	5000

Optics EXPRESS

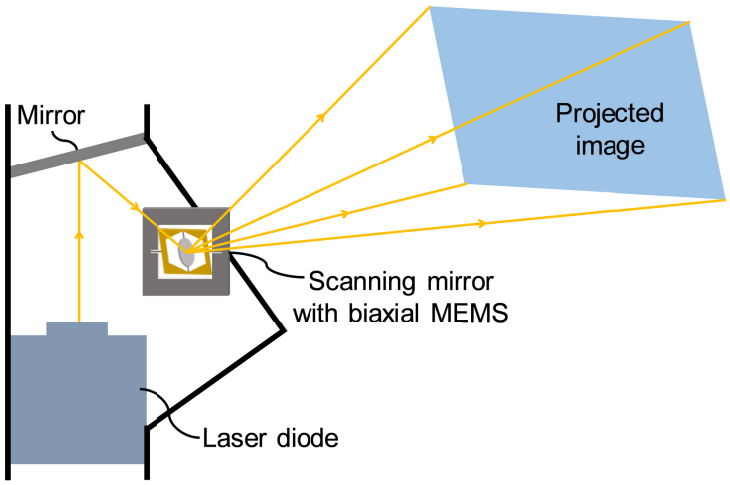

Fig. 5. Schematic drawing of the laser scanning projector, inside which are mounted a laser diode, a mirror, and a scanning mirror controlled by a biaxial MEMS.

2.4 Diffractive optical element

DOE is an array of diffraction gratings, the number of which shall match with the resolution of laser scanning projector. The size of each diffraction grating shall match with that of the beam emerging from MEMS, *i.e.* 60 μm. For enhancing the diffraction efficiency (DE) and eliminating the undesired diffraction orders, each grating is designed to be a slanted grating [44], as depicted in Fig. 6, where p is the grating period, h_g the grating depth, w_g the grating width, and β the slant angle relative to the normal. In order for the image to be immune to the change in diopter of eye, all the diffracted beams are supposed to pass through the lens center. For a grating located at a distance x from the left edge of DOE, its period p, diffraction order m, wavelength λ, incident angle θ_i and diffraction angle θ_m should satisfy both the reflection grating equation [45], *i.e.*

$$p\left(\sin\theta_i - \sin\theta_m\right) = m\lambda \tag{5}$$

and the geometry (see Fig. 1) given by

$$\tan\theta_i = \frac{d_{doe} + x}{d_p} \tag{6}$$

and

$$\tan\theta_m = \frac{W/2 - x}{d_{lens}} \tag{7}$$

Optics EXPRESS

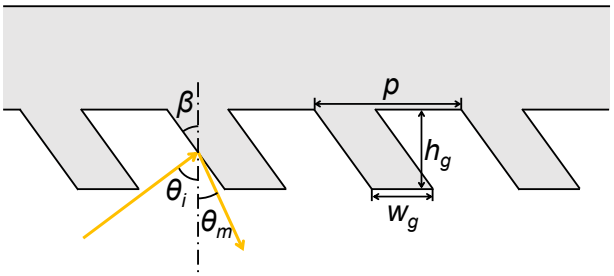

Fig. 6. Profile of the slanted grating, where p is the grating period, h_g the grating depth, w_g the grating width, β the slant angle relative to the normal, θ_i the incident angle, and θ_m the diffraction angle.

3. Results and discussion

3.1 Simulation setting

The performance of our RSD is quantitatively analyzed with Code V (Synopsys) and COMSOL Multiphysics (COMSOL). Capable of ray tracing, Code V lends itself to analyzing the imaging properties, such as modulation transfer function (MTF), distortion, and imaging simulation. Based on the finite element method [46], COMSOL Multiphysics is a powerful tool in dealing with the diffraction grating. The design wavelength is 532 nm.

Figure 7 outlines the optical surfaces used in Code V. The object is placed at 3 m ahead of the eye. Surfaces 1 to 8 (S1 to S8) constitute the moist eye, of which, S1 is tear, S2 anterior cornea, S3 posterior cornea, S4 iris with pupil, S5 anterior lens, S6 virtual plane, S7 posterior lens, and S8 retina. To imitate the laser scanning projector as a pinhole camera, the semi-aperture of virtual plane—where the lens center is located—is set as 30 μm, *i.e.* radius of the laser beam.

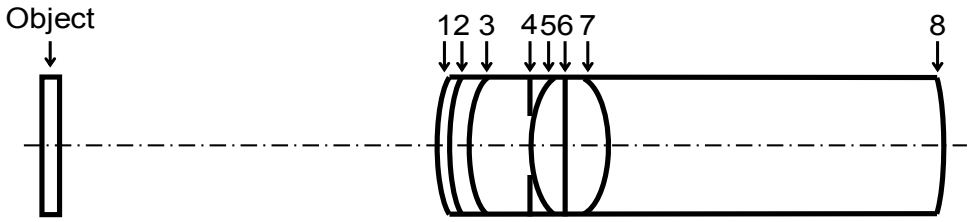

Fig. 7. Optical surfaces used in Code V. The object is placed at 3 m ahead of the eye. Surfaces 1 to 8 (S1 to S8) constitute the moist eye, of which, S1 is tear, S2 anterior cornea, S3 posterior cornea, S4 iris with pupil, S5 anterior lens, S6 virtual plane, S7 posterior lens, and S8 retina.

The original parameters of eye are adopted from [35], wherein the eye is focused to the infinity. In our model, with the tear being added and the object distance being assigned as 3 m, those parameters need to be tweaked through an optimization, which is carried out under a constraint that the length of eye be 24 mm [34]. As a result, Table 3 summarizes the optimized parameters, where AL and PL, in turn, denote the gradient refractive indices of anterior and posterior lenses. Besides, detailed parameters for aspherical surfaces and gradient lens are provided in Table 4 and Table 5, respectively.

Optics EXPRESS

Table 3. Parameters of optical surfaces used in Code V

Surface	Surface type	Radius (mm)	Thickness (mm)	Refractive index[a]	Semi-aperture (mm)
object	sphere	infinity	3000		
1 (tear)	asphere	7.7600	0.0130[b]	1.340	4.9510
2 (anterior cornea)	asphere	7.7600	0.5500	1.376	4.9344
3 (posterior cornea)	asphere	6.5200	3.0500	1.336	4.3777
4 (iris with pupil)	sphere	infinity	0	1.336	2.2928
5 (anterior lens)	asphere	14.3669	1.7136	AL[c]	2.0569
6 (virtual plane)	sphere	infinity	1.3522	PL[d]	0.0300[e]
7 (posterior lens)	asphere	–7.0081	17.3213	1.336	1.5423
8 (retina)	sphere	–13.0000	0.0000	1.336	12.5647

[a]Refractive index of air is left empty. [b]Thickness of tear usually ranges from 6 to 20 μm [37]. [c]AL denotes the gradient refractive indices of anterior lens. [d]PL denotes the gradient refractive indices of posterior lens. [e]The semi-aperture of virtual plane—where the lens center is located—is set as 30 μm, *i.e.* radius of the laser beam.

Table 4. Detailed parameters for aspherical surfaces

Surface	Y radius (mm)	Conic constant (K)	4^{th} order coefficient (A)	6^{th} order coefficient (B)
1 (tear)	7.76	–0.1	0	0
2 (anterior cornea)	7.76	–0.1	2.0e-5	0
3 (posterior cornea)	6.52	–0.3	–2.0e-5	0
5 (anterior lens)	14.37	–0.12	0.0012	–7.244e-5
7 (posterior lens)	–7.008	0.23	0.0005	4.320e-5

Table 5. Detailed parameters for gradient refractive indices of anterior and posterior lenses

Refractive index	n_{00}	c_{01}	c_{02}	c_{03}	c_{04}	c_{10}	c_{20}
Anterior lens	1.376	0.04292	–0.01001	–0.1929e-2	–0.707e-4	–0.1748e-2	0.2180e-4
Posterior lens	1.416	0	–0.4113e-2	0	–0.3318e-3	–0.1748e-2	0.2180e-4

3.2 Ray tracing diagram

Figure 8 shows the ray tracing diagram for the fields of 0°, 10°, 20°, 30°, 40°, 50°, and 61°, from which it can be seen that all rays are converged at the lens center.

Optics EXPRESS

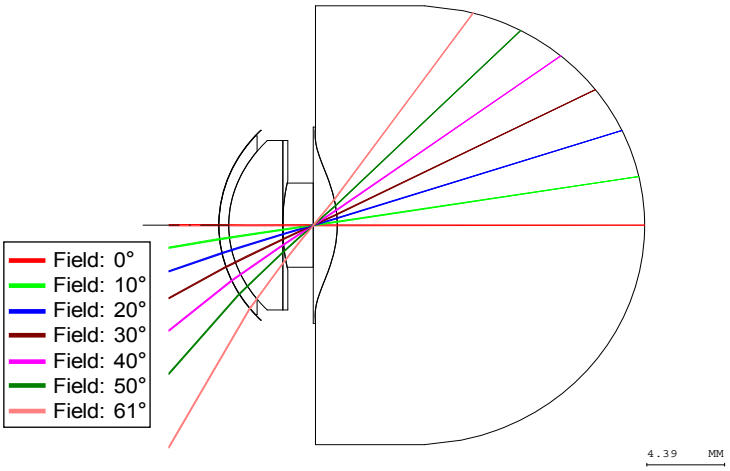

Fig. 8. Ray tracing diagram for the fields of 0°, 10°, 20°, 30°, 40°, 50°, and 61°. It can be seen that all rays are converged at the lens center.

3.3 Field of view

As illustrated in Fig. 9, FOV, whose vertex is situated at the center of entrance pupil, is the angle subtended by DOE. If measured diagonally, it could be determined by

$$FOV = 2\tan^{-1}\left(\frac{\sqrt{W^2+H^2}}{2\left(d_{er}+d_{ep}\right)}\right) \tag{8}$$

where H is the vertical dimension of DOE, d_{er} the eye relief, and d_{ep} the distance from the vertex of tear to the center of entrance pupil, which is calculated as 3.05 mm. Say $W = H =$ 38.4 mm and $d_{er} = 12$ mm, FOV is 122° (diagonal).

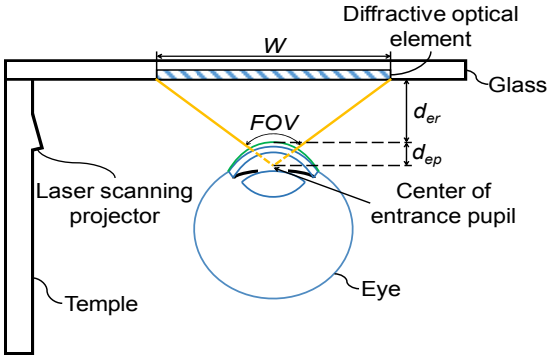

Fig. 9. Illustration of FOV, which is the angle subtended by DOE and whose vertex is situated at the center of entrance pupil. Say $W = H =$ 38.4 mm and $d_{er} =$ 12 mm, FOV is 122° (diagonal).

3.4 Angular resolution

Angular resolution (AR) in arcminute (′) is calculated by dividing FOV in degree (°) by the number of pixels N along the diagonal, which can be written as [47]

$$AR = \frac{60\cdot FOV}{N} = \frac{60\cdot FOV}{\sqrt{N_h^2+N_v^2}} \tag{9}$$

Optics EXPRESS

where N_h and N_v are the number of pixels along the horizontal and vertical directions, respectively. For FOV = 122°, N_h = 640, and N_v = 640, angular resolution 8.09′.

3.5 Diffraction efficiency and transmittance

In modeling the grating, wave optics module of COMSOL Multiphysics using the interface of electromagnetic wave, frequency domain is employed. The boundary condition is Floquet periodicity. The incident light is linearly polarized as transverse electric (TE) mode. The diffraction order m is + 1. The glass substrate of DOE is chosen as N-BK7 (Schott), whose refractive index is 1.5195 at 532 nm. Without loss of generality, 9 gratings are picked for simulation, as shown in Fig. 10. Say d_p = 10 mm, d_{doe} = 20 mm, and d_{lens} = 16.73 mm, according to Eqs. (5) and (6), the incident/diffraction angles θ_i/θ_m can be calculated. Based on the optimization, the optimal grating parameters, DEs, and transmittance T for normal incidence (θ_i = 0°) are obtained as in Table 6. The average DE and T are 57.6% and 80.6%, respectively.

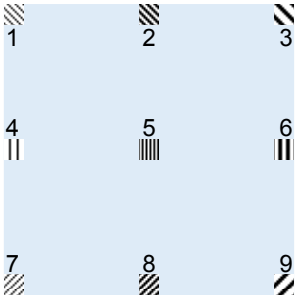

Fig. 10. 9 gratings picked for simulation, of which 1 is on the upper-left, 2 the upper-center, 3 the upper-right, 4 the middle-left, 5 the middle-center, 6 the middle-right, 7, the lower-left, 8 the lower-center, and 9 the lower-right.

Table 6. Optimized parameters of gratings

#	θ_i (°)	θ_m (°)	p (nm)	β (°)	w_g (nm)	h_g (nm)	DE (%)	T (%)
1	43.76	–34.34	423.6	52	163.8	500	57.61	62.26
2	59.9	–37.30	361.6	48	146.2	500	64.11	93.03
3	74.59	–55.55	297.4	40	119.6	500	59.21	98.42
4	63.43	48.93	3786.2	85	1327	500	58.42	79.78
5	75.69	0	549.0	63	218.0	500	52.20	39.76
6	80.28	–48.93	305.8	42	124.7	500	46.06	98.50
7	43.76	–34.34	423.6	52	163.8	500	57.61	62.26
8	59.9	–37.30	361.6	48	146.2	500	64.11	93.03
9	74.59	–55.55	297.4	40	119.6	500	59.21	98.42
						Average	57.62	80.61

3.6 Uniformity

As DE of each grating of DOE more or less differs, a figure of merit Γ to evaluate the uniformity is introduced as [20]

$$\Gamma = 1 - \frac{\sigma}{DE_{avg}} \tag{10}$$

where DE_{avg} is the average DE, and σ is the standard deviation formulated as

$$\sigma = \sqrt{\frac{1}{n}\sum_{i=1}^{n}\left(DE_i - DE_{avg}\right)^2} \tag{11}$$

Optics EXPRESS

where n is the number of gratings of interest, and i the serial number. Calculated with DEs listed in Table 6, the uniformity Γ is 0.91.

3.7 Luminance

Luminance is a measure of the luminous intensity per unit area of light that is diffracted from the DOE within the entire FOV. By this definition, we could express the luminance in terms of the luminous flux Φ, average DE DE_{avg} of DOE, solid angle Ω subtended by DOE, and area A of DOE, *i.e.*

$$L = \frac{\Phi \cdot DE_{avg}}{\Omega \cdot A} \tag{12}$$

where

$$\Omega = 4\cos^{-1}\sqrt{\frac{1+\left(\frac{W}{2d_{lens}}\right)^2+\left(\frac{H}{2d_{lens}}\right)^2}{\left[1+\left(\frac{W}{2d_{lens}}\right)^2\right]\left[1+\left(\frac{H}{2d_{lens}}\right)^2\right]}} \tag{13}$$

and

$$A = W \cdot H \tag{14}$$

When the luminous flux of projector is 2 lm, luminance is 323 cd/m^2 or nit.

3.8 Spot diagram

Figure 11 plots the spot diagram for the fields of 0°, 10°, 20°, 30°, 40°, 50°, and 61°, from which it can be seen that the spot of each field is smaller than the Airy disk.

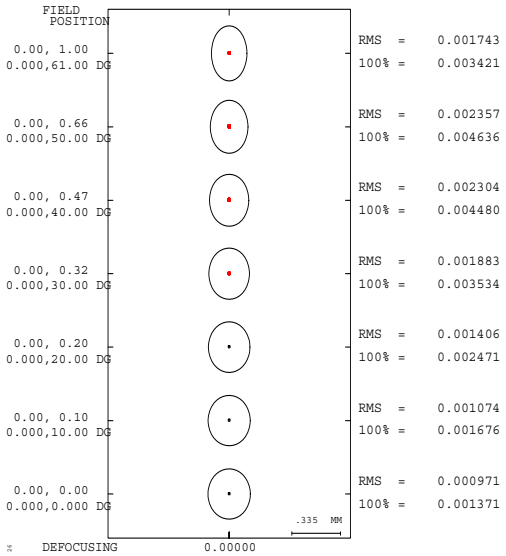

Fig. 11. Spot diagram for the fields of 0°, 10°, 20°, 30°, 40°, 50°, and 61°. It can be seen that the spot of each field is smaller than the Airy disk.

Optics EXPRESS

3.9 MTF

As shown in Fig. 12, MTFs are calculated as a function of spatial frequency in cycle/degree for the fields of 0° and 61° when the distances between DOE and eye are offset by 0 mm, 3 mm and 6 mm from the target eye relief of 12 mm, respectively. At 3.71 cycle/degree, which corresponds to the angular resolution of 8.09′, MTFs are above 0.99999 for all fields and eye relief offsets. This agrees with the foregoing statement on the laser scanning projector in analogy to a pinhole camera. This also indicates that even if the laser beams are not perfectly converged at the center of lens, the image quality will not be much affected.

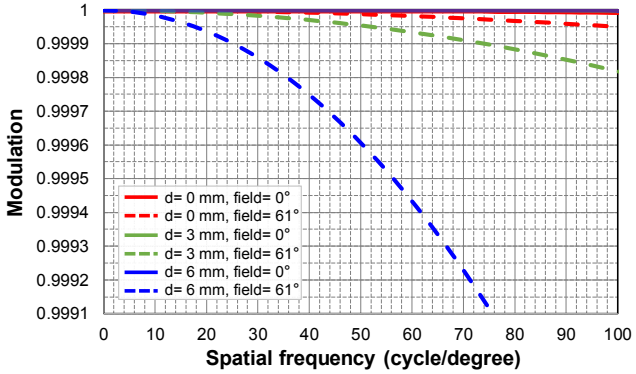

Fig. 12. MTFs are calculated as a function of spatial frequency in cycle/degree for the fields of 0° and 61° when the distances between DOE and eye are offset by 0 mm, 3 mm and 6 mm from the target eye relief of 12 mm, respectively. At 3.71 cycle/degree, which corresponds to the angular resolution of 8.09′, MTFs are above 0.99999 for all fields and eye relief offsets.

3.10 Contrast ratio

CR—the ratio of maximum intensity to minimum intensity [48]—can be deduced as

$$CR = \frac{CR_0 + 1 + MTF \cdot (CR_0 - 1)}{CR_0 + 1 - MTF \cdot (CR_0 - 1)} \tag{15}$$

where CR_p is the CR of laser scanning projector. For the field of 0°, CR_p = 5000, MTF = 0.99999, and CR = 4878.

3.11 Distortion

Distortion, which measures the difference between the paraxial and actual image heights, is defined as [49]

$$Distortion = \frac{h_a - h_p}{h_p} \tag{16}$$

where h_p is the paraxial image height calculated with the first-order approximation, and h_a is the actual image height. As the retina is a non-flat image surface, the chief ray shall be extended to intersect the flat paraxial image surface for calculating the image height. As can be seen in Fig. 13, the distortion is 24%, give or take.

Optics EXPRESS

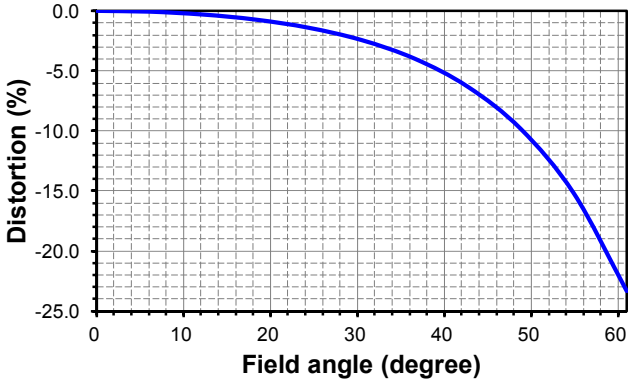

Fig. 13. Distortion versus the field angle. For the fact that the eye is far from being an ideal imaging system, distortion is an inherent characteristic of all retinal projection based NEDs.

3.12 Simulated imaging

Figure 14 shows the original image alongside the see-through retinal and projected retinal images. Compared to the original one, the projected retinal image is, while distorted, sharp and bright as a whole. In particular, the uncompromised brightness is extremely critical for the outdoors usage.

Fig. 14. (a) Original image (photographer: C. P. Chen, location: Duku Highway, Xinjiang, China), (b) see-through retinal image, and (c) projected retinal image. Compared to the original one, the projected retinal image is, while distorted, sharp and bright as a whole.

4. Conclusions

A lensless RSD and its working principles have been proposed. Its structure is highlighted by a laser scanning projector, a DOE, and a moist eye. To precisely model the eye, tear and gradient lens are taken into account. Based on the simulation, FOV is 122°, angular resolution is 8.09′, average DE of DOE is 57.6%, average transmittance of DOE is 80.6%, uniformity is 0.91, luminance is 323 cd/m^2, MTFs are above 0.99999 at 3.71 cycle/degree for all fields and offsets, CR is 4878, and distortion is 24%. As opposed to other retinal projection based NEDs [32–34], our RSD exhibits several unique features. First, no lens—except the lens of eye—is involved. Second, the projected retinal image is focus free. If constructed as a binocular RSD, it would be inherently free of the vergence-accommodation conflict [50]. Third, DOE is used as a combiner, making the device compact in design and suitable for see-through augmented reality. Fourth, the retinal image is immune to the change in the diopter of eye and pupil size. Instead, it will be subject to the rotation of eye, thereby fixating the eye to look straight ahead. That being said, a user can still look around by rotating his/her head if the head tracking is enabled.

Optics EXPRESS

Funding

National Natural Science Foundation of China (61831015); Science and Technology Commission of Shanghai Municipality (19ZR1427200, 1801H163000, 1701H169200); Shanghai Rockers Inc. (15H100000157).

Acknowledgments

Special thanks to Dr. Site Zhang (LightTrans, Germany) for his insightful comments on the manuscript.

References

1. J. E. Melzer and K. Moffitt, *Head-Mounted Displays: Designing for the User* (McGraw-Hill, 1997).
2. W. Barfield, *Fundamentals of Wearable Computers and Augmented Reality 2nd Edition* (Chemical Rubber Company, 2015).
3. M. S. Brennesholtz and E. H. Stupp, *Projection Displays 2nd Edition* (Wiley, 2008).
4. J. P. Rolland, "Wide-angle, off-axis, see-through head-mounted display," Opt. Eng. **39**(7), 1760–1767 (2000).
5. S. Liu, H. Hua, and D. Cheng, "A novel prototype for an optical see-through head-mounted display with addressable focus cues," IEEE Trans. Vis. Comput. Graph. **16**(3), 381–393 (2010).
6. H.-S. Chen, Y.-J. Wang, P.-J. Chen, and Y.-H. Lin, "Electrically adjustable location of a projected image in augmented reality via a liquid-crystal lens," Opt. Express **23**(22), 28154–28162 (2015).
7. R. Zhu, G. Tan, J. Yuan, and S.-T. Wu, "Functional reflective polarizer for augmented reality and color vision deficiency," Opt. Express **24**(5), 5431–5441 (2016).
8. L. Zhou, C. P. Chen, Y. Wu, Z. Zhang, K. Wang, B. Yu, and Y. Li, "See-through near-eye displays enabling vision correction," Opt. Express **25**(3), 2130–2142 (2017).
9. Q. Gao, J. Liu, X. Duan, T. Zhao, X. Li, and P. Liu, "Compact see-through 3D head-mounted display based on wavefront modulation with holographic grating filter," Opt. Express **25**(7), 8412–8424 (2017).
10. A. Maimone, A. Georgiou, and J. S. Kollin, "Holographic near-eye displays for virtual and augmented reality," ACM Trans. Graph. **36**(4), 85 (2017).
11. G.-Y. Lee, J.-Y. Hong, S. Hwang, S. Moon, H. Kang, S. Jeon, H. Kim, J.-H. Jeong, and B. Lee, "Metasurface eyepiece for augmented reality," Nat. Commun. **9**(1), 4562 (2018).
12. Y. Amitai, "Extremely compact high-performance HMDs based on substrate-guided optical element," in *SID Symposium Digest of Technical Papers* (2004), pp. 310–313.
13. T. Levola, "Diffractive optics for virtual reality displays," J. Soc. Inf. Disp. **14**(5), 467–475 (2006).
14. H. Mukawa, K. Akutsu, I. Matsumura, S. Nakano, T. Yoshida, M. Kuwahara, and K. Aiki, "A full-color eyewear display using planar waveguides with reflection volume holograms," J. Soc. Inf. Disp. **17**(3), 185–193 (2009).
15. D. Cheng, Y. Wang, H. Hua, and M. M. Talha, "Design of an optical see-through head-mounted display with a low f-number and large field of view using a freeform prism," Appl. Opt. **48**(14), 2655–2668 (2009).
16. Q. Wang, D. Cheng, Y. Wang, H. Hua, and G. Jin, "Design, tolerance, and fabrication of an optical see-through head-mounted display with free-form surface elements," Appl. Opt. **52**(7), C88–C99 (2013).
17. X. Hu and H. Hua, "High-resolution optical see-through multi-focal-plane head-mounted display using freeform optics," Opt. Express **22**(11), 13896–13903 (2014).
18. Y. Weng, D. Xu, Y. Zhang, X. Li, and S.-T. Wu, "Polarization volume grating with high efficiency and large diffraction angle," Opt. Express **24**(16), 17746–17759 (2016).
19. J. Yang, P. Twardowski, P. Gérard, and J. Fontaine, "Design of a large field-of-view see-through near to eye display with two geometrical waveguides," Opt. Lett. **41**(23), 5426–5429 (2016).
20. Y. Wu, C. P. Chen, L. Zhou, Y. Li, B. Yu, and H. Jin, "Design of see-through near-eye display for presbyopia," Opt. Express **25**(8), 8937–8949 (2017).
21. Y. Wu, C. P. Chen, L. Zhou, Y. Li, B. Yu, and H. Jin, "Near-eye display for vision correction with large FOV," in *SID Display Week* (2017), pp. 767–770.
22. Z. Liu, Y. Pang, C. Pan, and Z. Huang, "Design of a uniform-illumination binocular waveguide display with diffraction gratings and freeform optics," Opt. Express **25**(24), 30720–30731 (2017).
23. Wikipedia, "Virtual retinal display," https://en.wikipedia.org/wiki/ Virtual_retinal_display.
24. T. A. Furness III and J. S. Kollin, "Virtual retinal display," US Patent 5,467,104 (1992).
25. S. C. McQuaide, E. J. Seibel, J. P. Kelly, B. T. Schowengerdt, and T. A. Furness III, "A retinal scanning display system that produces multiple focal planes with a deformable membrane mirror," Displays **24**(2), 65–72 (2003).
26. R. B. Sprague, "Method and apparatus to process display and non-display information," US Patent 8,520,309 B2 (2008).
27. R. Sprague, A. Zhang, L. Hendricks, T. O'Brien, J. Ford, E. Tremblay, and T. Rutherford, "Novel HMD concepts from the DARPA SCENICC program," Proc. SPIE **8383**, 838302 (2012).
28. A. Maimone, D. Lanman, K. Rathinavel, K. Keller, D. Luebke, and H. Fuchs, "Pinlight displays: wide field of view augmented reality eyeglasses using defocused point light sources," ACM Trans. Graph. **33**(4), 89 (2014).
29. E. Tremblay, M. Guillaumee, and C. Moser, "Method and apparatus for head worn display with multiple exit pupils," US Patent 9,846,307 B2 (2017).

Optics EXPRESS

30. R. J. Jacobs, I. L. Bailey, and M. A. Bullimore, "Artificial pupils and Maxwellian view," Appl. Opt. **31**(19), 3668–3677 (1992).
31. H. K. Walker, W. D. Hall, and J. W. Hurst, *Clinical Methods: The History, Physical and Laboratory Examinations 3rd Edition* (Butterworth-Heinemann, 1990), Chap. 58.
32. C. P. Chen, L. Zhou, J. Ge, Y. Wu, L. Mi, Y. Wu, B. Yu, and Y. Li, "Design of retinal projection displays enabling vision correction," Opt. Express **25**(23), 28223–28235 (2017).
33. L. Mi, W. Zhang, C. P. Chen, Y. Zhou, Y. Li, B. Yu, and N. Maitlo, "A retinal-projection-based near-eye display for virtual reality," Proc. SPIE **10676**, 106761C (2018).
34. Y. Wu, C. P. Chen, L. Mi, W. Zhang, J. Zhao, Y. Lu, W. Guo, B. Yu, Y. Li, and N. Maitlo, "Design of retinal-projection-based near-eye display with contact lens," Opt. Express **26**(9), 11553–11567 (2018).
35. A. V. Goncharov and C. Dainty, "Wide-field schematic eye models with gradient-index lens," J. Opt. Soc. Am. A **24**(8), 2157–2174 (2007).
36. M. Bass, C. DeCusatis, J. Enoch, V. Lakshminarayanan, G. Li, C. MacDonald, V. Mahajan, and E. V. Stryland, *Handbook of Optics 3rd Edition Volume III: Vision and Vision Optics* (McGraw-Hill Education, 2009).
37. M. Farid, "The tear film: the neglected refractive interface," https://www.eyeworld.org/supplements/EW-September-supplement-2014.pdf.
38. Wikipedia, "Cardinal point (optics)," https://en.wikipedia.org/wiki/Cardinal_point_(optics).
39. S. E. Lyshevski, *Nano- and Micro-Electromechanical Systems: Fundamentals of Nano- and Microengineering 2nd Edition* (Chemical Rubber Company, 2005).
40. F. L. Pedrotti, L. M. Pedrotti, and L. S. Pedrotti, *Introduction to Optics 3rd Edition* (Pearson, 2006).
41. https://www.projectorcentral.com/Microvision-projectors.htm.
42. O. Svelto, *Principles of Lasers 5th Edition* (Springer, 2010).
43. B. Redding, M. A. Choma, and H. Cao, "Speckle-free laser imaging using random laser illumination," Nat. Photonics **6**(6), 355–359 (2012).
44. T. Levola and P. Laakkonen, "Replicated slanted gratings with a high refractive index material for in and outcoupling of light," Opt. Express **15**(5), 2067–2074 (2007).
45. E. G. Loewen and E. Popov, *Diffraction Gratings and Applications* (Marcel Dekker, 1997).
46. COMSOL, "An introduction to the finite element method," https://www.comsol.com/multiphysics/finite-element-method.
47. W. Zhang, C. P. Chen, L. Mi, Y. Lu, M. Zhu, X. Ren, R. Tang, and N. Maitlo, "A retinal-projection-based near-eye display with contact lens for mixed reality," Proc. SPIE **11040**, 1104005 (2019).
48. L. Mi, C. P. Chen, Y. Lu, W. Zhang, M. Zhu, R. Tang, X. Ren, and N. Maitlo, "A lensless retinal scanning display for augmented reality," in *SID Display Week* (2019), pp. 1583–1586.
49. R. E. Fischer, B. Tadic-Galeb, and P. R. Yoder, *Optical System Design 2nd Edition* (McGraw-Hill Education, 2008).
50. H. Hua, "Enabling focus cues in head-mounted displays," Proc. IEEE **105**(5), 805–824 (2017).